12th INTERNATIONAL SCIENTIFIC CONFERENCE ON DEFENSIVE TECHNOLOGIES
OTEH 2026
Serbia, Tara, 21 - 24 October 2026

SHEAR STRESS-BASED FORCE MODELING FOR M-84 TRACKED VEHICLE ON DEFORMABLE TERRAIN

MOMIR DRAKULIĆ
University of Defence in Belgrade, Military Academy, Belgrade, momir.drakulic@va.mod.gov.rs

ALEKSANDAR ĐURIĆ
University of Defence in Belgrade, Military Academy, Belgrade, aleksandar.djuric@va.mod.gov.rs

Abstract: *This paper presents a methodology for calculating interaction forces acting on the tracked armoured vehicle M-84 during motion on deformable terrain. The research is based on a previously developed and experimentally validated track-terrain interaction model, which is extended toward application at the vehicle level. The proposed approach applies a shear stress model within the framework of terramechanics theory to estimate the distribution of stresses along the track-soil contact area. Based on this model, the resultant interaction forces are numerically evaluated under different operating conditions, including straight motion and steering. The calculated force outputs are structured for integration into a complete dynamic vehicle model. They also provide a consistent input set for driveline analysis and transmission studies, especially for optimization of the gear shifting process in a power-shift transmission system, aiming to achieve smooth gear transitions without interruption of power flow. The presented methodology contributes to improved prediction of mobility performance and supports further development of control-oriented models of tracked armoured vehicles.*

Keywords: *Tracked vehicle, terramechanics, shear stress model, track-soil interaction, vehicle dynamics.*

1. INTRODUCTION

Tracked vehicles are designed to maintain mobility across terrains that vary significantly in stiffness, strength, and surface conditions [1,2]. Their operational performance depends not only on propulsion and suspension systems but also on the complex mechanics of track–terrain interaction [3,4]. During high-speed steering manoeuvres, nonlinear distributions of contact forces emerge, which strongly affect vehicle stability, controllability, and energy consumption [5]. These effects become especially pronounced in heavy platforms such as main battle tanks, where large inertial loads amplify slip, lateral displacement, and uneven load distribution along the track [6].

Accurate prediction of track–terrain interaction forces is essential for reliable assessment of vehicle behaviour under demanding operating conditions [7]. Empirical models provide simplified estimates but often fail to capture the coupled effects of soil deformation and slip dynamics [8]. On the other hand, high-fidelity numerical methods, such as discrete element or finite element approaches, offer improved physical realism but are typically computationally expensive for system-level simulations. Therefore, a balanced modelling approach that combines physical consistency with computational efficiency is required for engineering analysis and design purposes.

The simulation framework used in this study is based on terramechanics principles and the shear stress theory of soil deformation, enabling the prediction of longitudinal and lateral contact forces generated during track–terrain interaction [9]. The model has previously been developed and validated for the infantry fighting vehicle BVP M80, with results reported in [10], where good agreement with experimental data was demonstrated in terms of contact force distribution and vehicle trajectory prediction.

In this work, the same validated modelling framework is applied to the M84 main battle tank. The objective is to investigate how changes in vehicle mass, geometry, and inertial properties influence the predicted track–terrain interaction forces during steering manoeuvres. By introducing vehicle-specific parameters, the study evaluates the adaptability of the model to a heavier and dynamically different tracked platform, while maintaining the same underlying physical formulation.

The contribution of this paper lies in demonstrating the transferability of a previously validated terramechanics-based simulation model to a different class of tracked vehicle and in analysing the resulting differences in contact force distribution under identical maneuver conditions. The results provide additional insight into the influence of vehicle configuration on track–terrain interaction and support the use of such models in comparative studies, system design, and further development of control-oriented simulation tools.

2. MODELING

Considering the variety of approaches used in the analysis of track–terrain interaction, a systematic overview of modern terramechanics methods is given in [8,11]. To achieve a balance between physical realism, numerical stability, and computational efficiency, the Janosi–Hanamoto semi-empirical model is adopted as the basis for

Corresponding author: M. Drakulić;
E-mail: momir.drakulic@va.mod.gov.rs

DOI: 10.5937/OTEH26024D

describing the shear behaviour of deformable terrain. This choice is consistent with the modelling framework previously developed and validated in [10], where the same approach was successfully applied to the infantry fighting vehicle BVP M80.

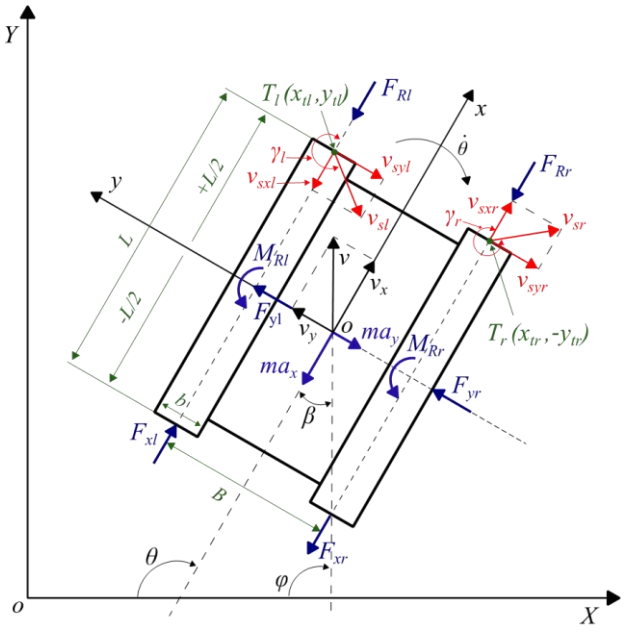


Figure 1. Tracked vehicle during the steering [10].

Starting from the established modelling framework, a consistent vehicle dynamics formulation is required to enable coupling with the terramechanics model [8,12,13]. The vehicle is considered as a rigid body performing planar motion during steering, where the interaction between the left and right track systems generates longitudinal and lateral motion as well as yaw dynamics. A detailed derivation of the governing equations of motion is provided in [10] and is directly utilized in the present study without modification of the underlying structure.

Within the Janosi–Hanamoto formulation, the key coupling variable between vehicle kinematics and soil response is the shear displacement, which arises due to the relative motion between the track and the deformable soil [14,15]. This quantity governs the development of shear stress within the contact patch and provides a direct link between slip conditions and traction generation. The shear stress is described by the exponential relationship:

$$\tau = (c + \sigma tan\phi)\left(1 - e^{-\frac{j}{K}}\right) \quad (1)$$

where c is the soil cohesion, σ is the normal stress, φ is the internal friction angle, j is the shear displacement, and K is the shear deformation modulus.

Based on the obtained shear stress distribution, the interaction forces between the track and the terrain are determined by integrating the local stresses over the contact length. In this way, the longitudinal and lateral force components acting on the right and left track are obtained as functions of vehicle motion, soil properties, and local pressure distribution [16–18].

Based on Figure 1, F_{xr} and F_{xl} represent the components of the shear force exerted by the right and left tracks, respectively, on the terrain in the x-direction. F_{yr} and F_{yl} are the corresponding components of the shear force in the y-direction. M_{Rr} and M_{Rl} denote the steering resistance torques for the right and left tracks, respectively, while F_{Rr} and F_{Rl} represent the rolling resistances for the tracks on both sides.

$$F_{xr} = \int_{-\frac{L}{2}}^{\frac{L}{2}} (c + p_r \tan\phi)\left(1 - e^{-\frac{j_r}{K}}\right) b\cos(\gamma_r + \pi)dx \quad (2)$$

$$F_{xl} = \int_{-\frac{L}{2}}^{\frac{L}{2}} (c + p_l tan\phi)\left(1 - e^{-\frac{j_l}{K}}\right) b\cos(\gamma_l + \pi)dx \quad (3)$$

$$F_{yr} = \int_{-\frac{L}{2}}^{\frac{L}{2}} (c + p_r tan\phi)\left(1 - e^{-\frac{j_r}{K}}\right) b\sin(\gamma_r + \pi)dx \quad (4)$$

$$F_{yl} = \int_{-\frac{L}{2}}^{\frac{L}{2}} (c + p_l tan\phi)\left(1 - e^{-\frac{j_l}{K}}\right) b\sin(\gamma_l + \pi)dx \quad (5)$$

In addition to traction forces, the model accounts for rolling resistance effects through a load-dependent formulation that includes lateral load transfer during steering manoeuvres. The normal load distribution between the left and right tracks is influenced by vehicle mass, lateral acceleration, centre of mass height, and track gauge, which leads to asymmetric resistance forces on the two sides of the vehicle [19]. This effect is incorporated in the form of equivalent resistance forces acting at the track level, ensuring compatibility with the overall dynamic equilibrium.

$$F_{Rr} = f\left(\frac{mg}{2} + \frac{ma_y h}{B}\right) \quad (6)$$

$$F_{Rl} = f\left(\frac{mg}{2} - \frac{ma_y h}{B}\right) \quad (7)$$

$$M_{Rr} = \int_{-\frac{L}{2}}^{\frac{L}{2}} (c + p_r tan\phi)\left(1 - e^{-\frac{j_r}{K}}\right) b\sin(\gamma_r + \pi)xdx \quad (8)$$

$$M_{Rl} = \int_{-\frac{L}{2}}^{\frac{L}{2}} (c + p_l tan\phi)\left(1 - e^{-\frac{j_l}{K}}\right) b\sin(\gamma_l + \pi)xdx \quad (9)$$

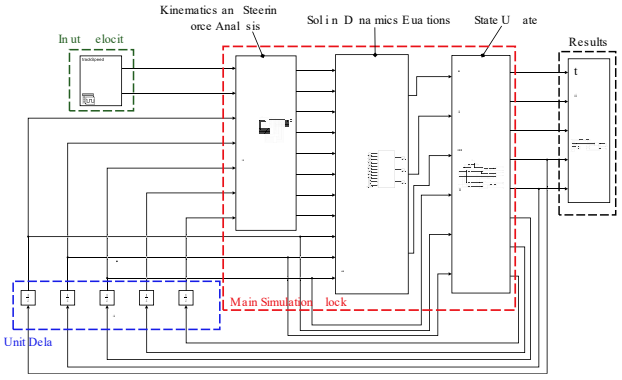


Figure 2. Simulation model [10].

The developed force and moment model is implemented in a MATLAB/Simulink environment, where it is coupled with the previously established vehicle dynamics model. The simulation structure enables numerical evaluation of high-speed steering manoeuvres by computing

instantaneous track–terrain interaction forces and vehicle response in a time-domain framework. Compared to the previously published model in [10], the present implementation retains the same mathematical structure while extending its application to a different vehicle class by introducing the geometric and inertial parameters of the M84 main battle tank, shown in table 1.

Table 1. Vehicle Parameters.

P me e	*V e*	*Uni*
m	13 850	[k]
L	3.3	[m]
B	2.526	[m]
b	0.31	[m]
h	1.139	[m]
	0.258	[m]
i	5.786	–

3. RESULTS

For the purposes of simulation, a Gault clay soil was selected as the terrain type (Table 2), as it is representative of cohesive soil conditions commonly associated with the operational environments of the M84 tracked vehicle. The reference trajectory to be followed by the vehicle was predefined [20,21], and a closed-loop control structure based on a PID controller was implemented to ensure accurate trajectory tracking. The controller continuously minimizes the position error between the desired and actual vehicle path, thereby enabling the system to follow the prescribed trajectory while maintaining stable dynamic response throughout the maneuver. The simulated trajectory, shown in Figure 3, closely follows the prescribed reference path throughout the entire manoeuvre.

Table 2. Terrain Parameters.

P me e	*G*	*Uni*
c	68.92	[kPa]
φ	34	[^{0}]
K	0.6	[cm]

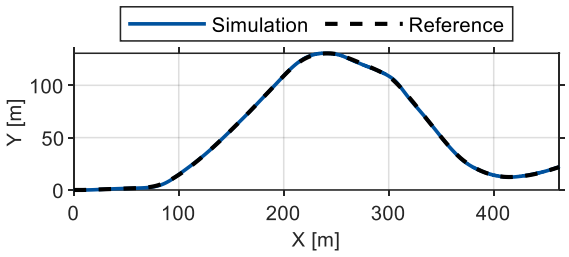


Figure 3. Vehicle trajectory.

This confirms that the PID-based closed-loop control structure maintains adequate path-tracking accuracy despite the combined influence of nonlinear shear-stress traction forces and lateral load transfer acting on the vehicle.

The corresponding sideslip angle, presented in Figure 4, remains within a narrow ran e of a roximatel −0.4° to +0.2°, with the most pronounced excursions coinciding with the steepest curvature segments of the trajectory (aroun t ≈ 10 s an t ≈ 40–55 s). This behaviour confirms the expected coupling between path curvature and lateral slip and indicates that lateral instability effects remain limited for the considered manoeuvre and terrain conditions.

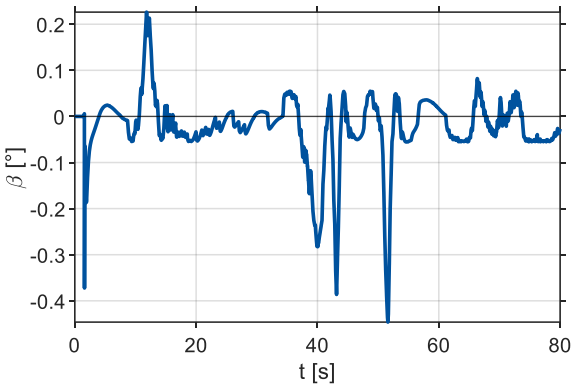


Figure 4. Sideslip angle.

This kinematic response is governed by the underlying track–terrain interaction forces. The longitudinal forces on the right and left track, shown in Figures 5 and 6 respectively.

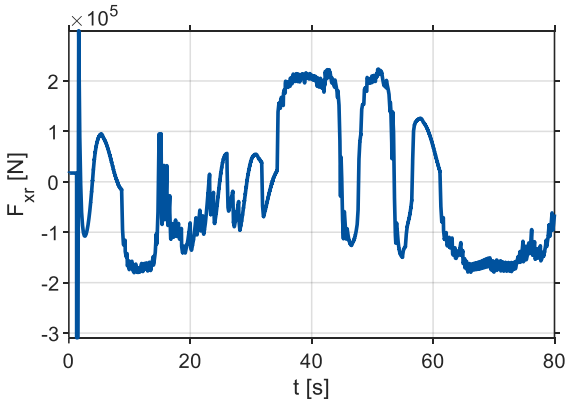


Figure 5. Longitudinal force on the right track.

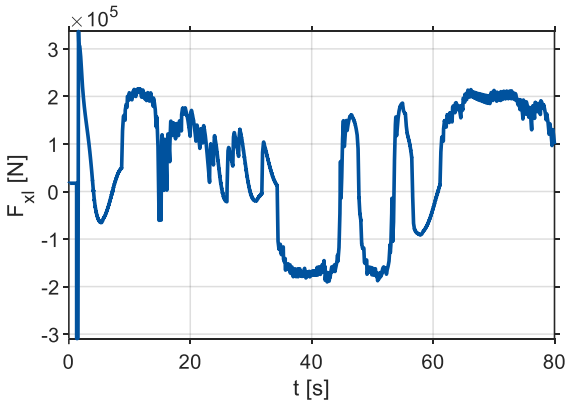


Figure 6. Longitudinal force on the left track.

This asymmetry between Fxr and Fxl is consistent with the

differential traction and braking distribution required for skid-steering and represents the primary mechanism generating the yaw moment needed to execute the prescribed turn; the pronounced plateau visible between t ≈ 30–55 s corresponds to the sustained turning phase, during which the outer track is required to sustain a higher traction level than the inner track.

A similar coupling is observed in the lateral force components, presented in Figures 7 and 8, which remain close to zero during straight-line motion and develop pronounced peaks of up to approximately 3.5×10^4 N urin the steering phase.

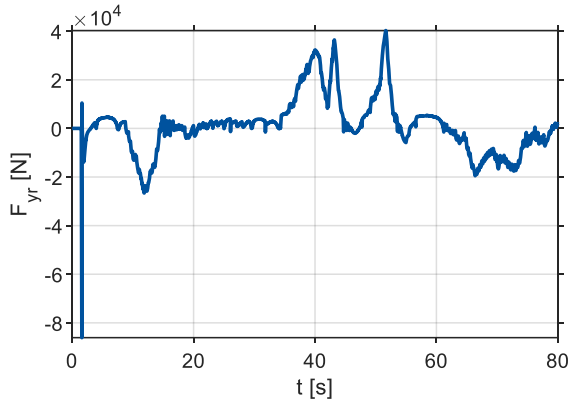


Figure 7. Lateral force on the right track.

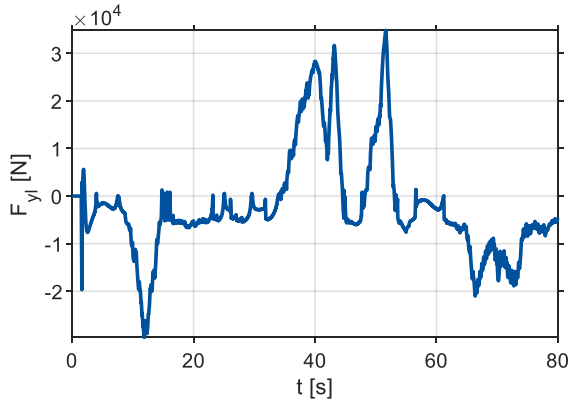


Figure 8. Lateral force on the left track.

The magnitude and timing of these lateral force peaks correlate well with the sideslip angle response discussed above, confirming the physical consistency of the shear-stress-based lateral force formulation across both tracks. The combined effect of these longitudinal and lateral force asymmetries is reflected in the turning resistance moment shown in Figure 9, which varies between approximately -5×10^5 Nm an 5×10^5 Nm and reaches its largest sustained values during the central turning segment of the manoeuvre; the relatively high magnitude of this moment, compared with the values previously reported for the lighter BVP M80 platform in [10], illustrates the influence of the M-84's larger mass and track gauge on rolling and turning resistance.

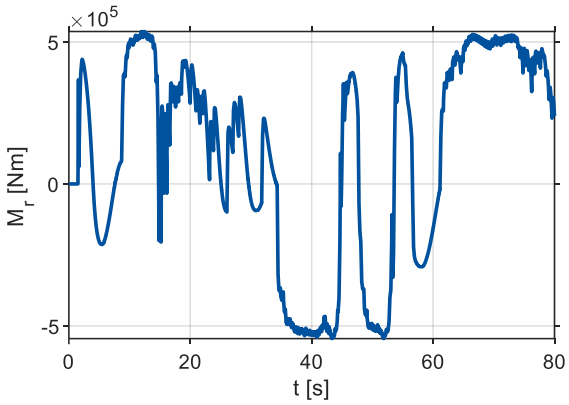


Figure 9. Turning resistance moment.

Despite these substantial variations in track forces and moments, the vehicle's speed response remains well-regulated. Following an initial transient associated with the start of the manoeuvre, the total vehicle speed, shown in Figure 10, stabilises around 25 km/h with only minor fluctuations of approximately ±1 km/h during the steering phase.

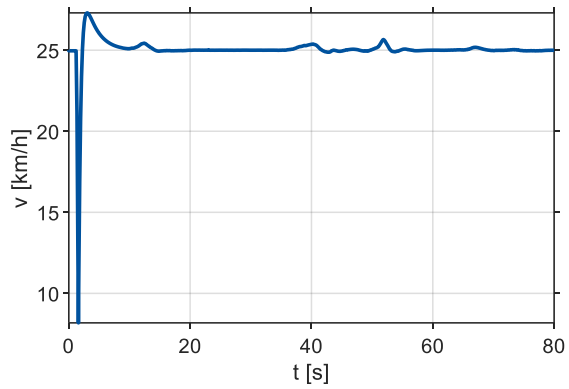


Figure 10. Total vehicle speed.

The longitudinal velocity component, presented in Figure 11, closely tracks this overall speed profile, confirming that the lateral velocity contribution remains small throughout the manoeuvre.

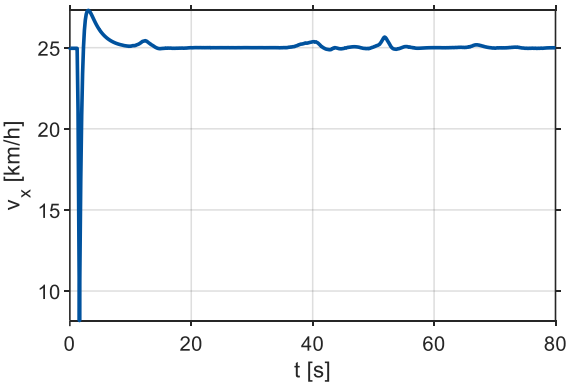


Figure 11. Longitudinal vehicle speed.

This is corroborated by the lateral velocity response in Figure 12, which stays within a narrow band of approximately ±0.15 km/h; although small in absolute terms, the visible oscillations during the steering phase are

directly linked to the lateral force and sideslip behaviour discussed above and represent the residual lateral dynamics not fully suppressed by the trajectory controller.

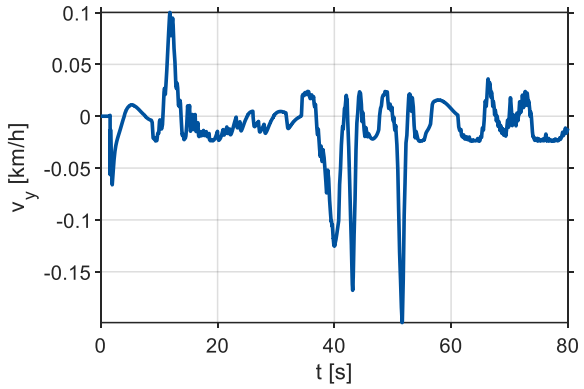


Figure 12. Lateral vehicle speed.

The corresponding acceleration responses further support this picture of stable, well-controlled vehicle behaviour. Apart from an initial transient peak of approximately 1.5 m/s² associated with the vehicle's start-up phase, the longitudinal acceleration in Figure 13 remains close to zero, with only minor oscillations occurring during the steering segment as the controller works to maintain constant forward speed under varying traction demand.

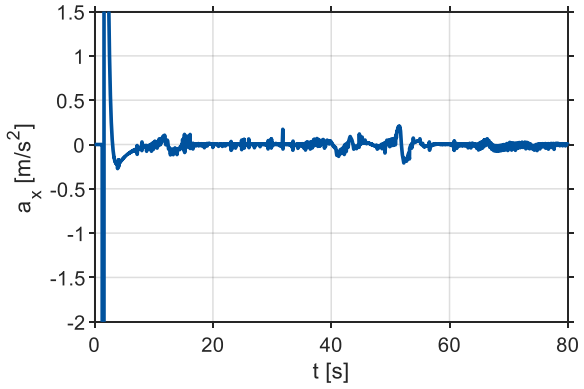


Figure 13. Longitudinal vehicle acceleration.

The lateral acceleration, shown in Figure 14, reaches peak values of approximately ±1.1 m/s² during the sharpest turning segments, in direct correspondence with the lateral force peaks discussed for Figures 7 and 8, these values remain within a range that does not indicate critical lateral instability, further supporting the conclusion that the controller and the underlying force model produce physically consistent vehicle behaviour.

Finally, the trajectory tracking error, presented in Figure 15, oscillates within approximately ±0.6 m, with the largest transient excursions occurring during the most demanding curvature changes of the manoeu re (t ≈ 15 s, 40 s an 50 s). While these peaks indicate a temporary degradation of tracking accuracy under high lateral force demand, the error consistently returns toward zero, confirming the overall stability and adequacy of the PID control structure for the considered class of high-speed steering manoeuvres.

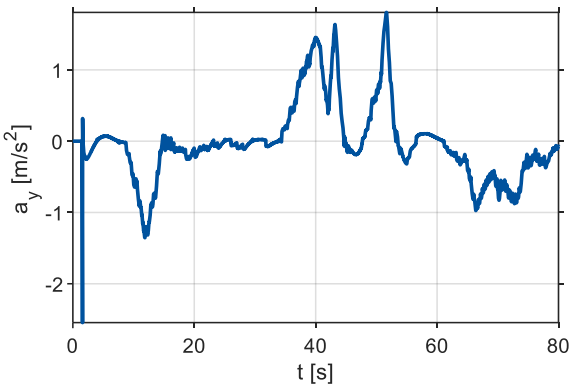


Figure 14. Lateral vehicle acceleration.

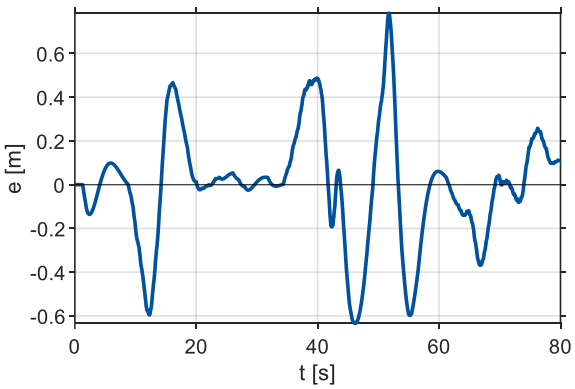


Figure 15. Trajectory tracking error.

4. CONCLUSION

This paper presented a shear stress-based methodology for calculating track–terrain interaction forces acting on the M-84 main battle tank during steering manoeuvres on deformable terrain. The approach extends a previously developed and experimentally validated terramechanics model, originally established for the infantry fighting vehicle BVP M80, to a heavier and dynamically different tracked platform by introducing the M-84's specific geometric and inertial parameters.

The simulation results, obtained for a representative cohesive soil (Gault clay) and a closed-loop PID-controlled steering manoeuvre, demonstrate that the model produces physically consistent and well-correlated force, moment, velocity and acceleration responses. The vehicle maintained accurate trajectory tracking, with sideslip angle and lateral acceleration remaining within bounded, stable ranges throughout the manoeuvre, while the trajectory tracking error remained limited even during the most demanding curvature transitions. The obtained results confirm the model's transferability across vehicle classes while preserving the same underlying physical formulation validated in [10].

The calculated force and moment outputs provide a consistent and structured data set suitable for integration into a complete vehicle dynamics model, and for driveline and transmission studies, including the optimisation of gear-shifting strategies in power-shift transmission

systems. Future work will focus on the experimental validation of the model for the M-84 platform, the extension of the analysis to additional terrain types and manoeuvre conditions, and a direct quantitative comparison between the M-84 and BVP M80 force responses to further characterise the influence of vehicle mass and geometry on track–terrain interaction.

Acknowledgments

This work was supported by the Ministry of Defense, Serbia, under the project „Modeling of Automotive Vehicle Assemblies for the Optimization of Dynamic Parameters", No. A -TT/1/26-28.

References

[1] Wong JY. Theory of ground vehicles. John Wiley & Sons; 2008.

[2] Wong JY. Terramechanics and off-road vehicle engineering: Terrain behaviour, off-road vehicle performance and Design. Elsevier; 2010.

[3] Garber M, Wong JY. Prediction of ground pressure distribution under tracked vehicles—II. Effects of design parameters of the track-suspension system on ground pressure distribution. Journal of Terramechanics 1981;18:71–9. https://doi.org/10.1016/0022-4898(81)90001-X.

[4] Tao J, Deng Z, Cao X, Hu G, Wang P. Modeling and Dynamic Characteristics of Tracked Vehicle Equipped with Symmetrical Suspensions Based on Multi-Body Dynamics and Discrete Element Coupling Method. Applied Sciences 2024;14:10618. https://doi.org/10.3390/app142210618.

[5] Golanbari B, Mardani A, Hosainpour A, Taghavifar H. Predicting terrain deformation patterns in off-road vehicle-soil interactions using TRR algorithm. Journal of Terramechanics 2024;117:101021. https://doi.org/10.1016/j.jterra.2024.101021.

[6] Lv G, Lv H, Chen Z, Chu W, Mao J. Research on inertia transfer in load simulation of tracked vehicle under complex working conditions. Front Mater 2023;10:1188411. https://doi.org/10.3389/fmats.2023.1188411.

[7] Öz emir MN, Kılıç , Ünlüso YS. A new contact & slip model for tracked vehicle transient dynamics on hard ground. Journal of Terramechanics 2017;73:3–23. https://doi.org/10.1016/j.jterra.2017.07.001.

[8] Chakravarthy PN, Sharma PK. Terramechanics Models for Tracked Vehicle Terrain Interaction Analysis A Review. Defence Science Journal 2024;74:469–81. https://doi.org/10.14429/dsj.74.19029.

[9] Janarthanan B, Padmanabhan C, Sujatha C. Lateral dynamics of single unit skid-steered tracked vehicle. International Journal of Automotive Technology 2011;12:865–75. https://doi.org/10.1007/s12239-011-0099-4.

[10] Drakulic M, Peric S, Djuric A, Rakic S. Track–terrain interaction during steering of high-speed tracked vehicles: Numerical modeling and experimental validation. Measurement 2025;256:118225. https://doi.org/10.1016/j.measurement.2025.118225.

[11] Jia W, Liu X, Zhang C, Qiu M, Tan Y, Yu Z. Design of Zero-Differential steering Controller for tracked vehicles with Hydraulic-Mechanical transmission based on particle swarm optimization Algorithm. IEEE Access 2023;11:32187–200. https://doi.org/10.1109/access.2023.3262515.

[12] Gorsich D, Vantsevich V, Paldan J, Moradi L. Modelling and simulation fundamentals in design for ground vehicle mobility Part II: Western approach. Journal of Terramechanics 2024;117:101023. https://doi.org/10.1016/j.jterra.2024.101023.

[13] Vantsevich V, Gorsich D. Modeling and simulation fundamentals in design for ground vehicle mobility part I: Eastern approach. Journal of Terramechanics 2024;117:101020. https://doi.org/10.1016/j.jterra.2024.101020.

[14] Ali Shaikh S, Li Y, Ma Z, Ali Chandio F, Hussain Tunio M, Ahmad F, et al. Effects of soil mechanical properties on the height and tractive performance of rubber grouser at different moisture contents. International Journal of Agricultural and Biological Engineering 2022;15:31–7. https://doi.org/10.25165/j.ijabe.20221506.7137.

[15] Meywerk M, Fortmüller T, Fuhr B, Baß S. Real-time model for simulating a tracked vehicle on deformable soils. Advances in Mechanical Engineering 2016;8:168781401664788. https://doi.org/10.1177/1687814016647889.

[16] Tota A, Galvagno E, Velardocchia M. Analytical study on the cornering behavior of an articulated tracked vehicle. Machines 2021;9:38. https://doi.org/10.3390/machines9020038.

[17] Tota A, Velardocchia M, Rota E, Novara A. Steering behavior of an articulated amphibious All-Terrain tracked vehicle. SAE Technical Papers on CD-ROM/SAE Technical Paper Series 2020. https://doi.org/10.4271/2020-01-0996.

[18] Dimauro L, Venturini S, Tota A, Galvagno E, Velardocchia M. High-speed tracked vehicle model order reduction for static and dynamic simulations. Defence Technology 2024;38:89–110. https://doi.org/10.1016/j.dt.2024.01.006.

[19] Garber M, Wong JY. Prediction of ground pressure distribution under tracked vehicles—I. An analytical method for predicting ground pressure distribution. Journal of Terramechanics 1981;18:1–23. https://doi.org/10.1016/0022-4898(81)90015-x.

[20] Drakulić M, Stanko ić M. ADRC-Based Trajectory Tracking of Unmanned Tracked Vehicles Under High Slippage Disturbance. 2024 14th International Conference on Electrical Engineering (ICEENG), IEEE; 2024, p. 362–6.

[21] Stankovic M, Ting H, Madonski R. From PID to ADRC an back: Ex ressin error-base acti e disturbance rejection control schemes as standard industrial 1DOF and 2DOF controllers. Asian Journal of Control 2024;26:2796–806. https://doi.org/10.1002/asjc.3373.